(Received 10 July 2025, Accepted 26 September 2025, Scheduled 24 December 2025)

Design of a High-Selectivity C-Band Tunable Filter by Dielectric Movable Elements for SATCOM Applications

dot(Davide Guarnera[1, *], Santi C. Pavone[1], Tommaso Isernia[2], and Gino Sorbello);[1]

[1] *Department of Electrical, Electronics, and Computer Engineering (DIEEI) University of Catania, Via Santa Sofia 64, Catania 95123, Italy*
[2] *Department of Information, Infrastructure and Sustainable Energy (DIIES) Mediterranea University of Reggio Calabria, Via Graziella Feo di Vito, Reggio Calabria 89122, Italy*

ABSTRACT: In this paper, the design of a mechanically tunable band-pass filter in waveguide technology operating in the C-band tunability range [4.4–5] GHz, for satellite communications (SATCOM), is presented. The resonance frequency tunability has been obtained by mechanically inserting movable dielectric cylinders within the waveguide filter. Impedance matching has been achieved by using two movable dielectric ridges, working as quarter-wave transformers. They have been placed at input and output filter ports and can move jointly with the dielectric tuning elements. Filter design has been carried out by adopting a suitable theoretical model, whereas the optimization has been achieved by numerical simulations. The proposed design approach provides key advantages in terms of simplicity, design effectiveness, and reproducibility, rendering it particularly suitable for industrial applications. A prototype of a high-selectivity tunable filter has been fabricated and characterized within the whole tunability range. The measurements show excellent agreement with simulated results.

1. INTRODUCTION

Microwave band-pass filters are essential components in satellite and, more broadly, wireless communication systems. In particular, the tunability of filter resonant frequency without significantly affecting the shape of frequency response (i.e., rigid translation of the frequency response) is mandatory in satellite, civil, and military applications [1–4]. This is because the channels within the passband are normally quite narrow and closely spaced each other. In this framework, tunable filters require high-selectivity in channel discrimination and accurate tunability, which are sometimes difficult to accomplish together.

Several techniques have been developed in the last few decades for the design of tunable microwave filters, which are summarized below, according to the exploited working principle:

- **Magnetically tunable filters:** They represent a widely used class of tunable filters. The principle of operation is based on devices with specific magnetic response, such as ferromagnetic devices, yttrium-iron garnet (YIG) resonators, or ferrite plates [5–7].
- **Electronically tunable filters:** Another class of tunable filters whose operation involves the use of active devices — such as pin diodes and varactors — to modify the filter network to achieve the desired frequency shift. Electronically tunable filters are characterized by high tuning ranges, but are not suitable for applications in which power handling capability is required [8–12].
- **Mechanically tunable filters:** These tunable filters work by modifying some geometrical or physical characteristics of the structure, usually through the insertion or displacement of metallic/dielectric elements, or by employing movable walls, to vary the resonance frequency. They are of interest in several applications, including those requiring high power handling capability [1, 13]. This category includes coaxial filters [14–17] and waveguide filters [18–21], both suitable for high-power operation. The latter are of particular importance in SATCOM transmitters, where input powers of the order of kilowatts are often required, and are widely employed thanks to their low losses and robustness.

The aim of this work is to present the design of a high-selectivity mechanically tunable filter in waveguide technology for C-band SATCOM applications, designed to operate within the tunability range [4.4–5] GHz ($\approx$ 12.8%). The adopted design technique is based on the dynamic modification of the guided wavelength inside a rectangular waveguide through the precisely controlled insertion of dielectric cylinders made of *alumina*, selected for its high power-handling capability [22, 23]. These cylinders act as periodic, tunable shunt reactive loads in the equivalent transmission-line model which describes the field propagation along the waveguide. Moreover, a reconfigurable matching network has been designed using movable quarter-wavelength dielectric ridges, which move in conjunction with the periodic arrangement of dielectric cylinders. This allows dynamically adapting the impedance matching network to the different equivalent loads exhibited by the various filter configurations.

* Corresponding author: Davide Guarnera (davide.guarnera@unict.it).

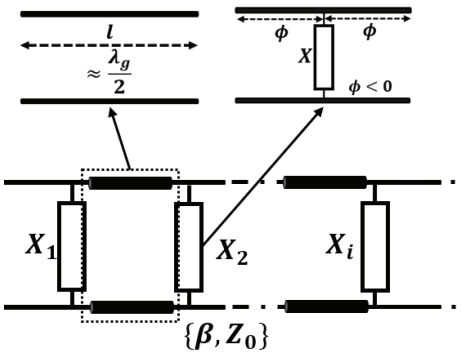

FIGURE 1. Equivalent transmission line model of the filter. According to this model, the filter cavities are represented as resonant transmission line sections of length $l_i \approx \lambda_g/2$, which correspond to series LC resonators in the equivalent circuital model. The cavities are coupled through inductive or capacitive irises, which work as impedance (admittance) inverters. These elements enable the realization of a ladder network composed of series and shunt LC resonators. In the equivalent circuit model, the irises are represented by shunt reactive loads (X) and transmission line sections with a negative equivalent electrical length (ϕ).

The proposed approach achieves high-performance tunable filters while maintaining simplicity and reproducibility, which are particularly valuable for industrial applications. Resonant cavity tunability is achieved by decoupling it from impedance matching requirements, which are addressed separately using a movable quarter-wavelength matching section. This approach introduces flexibility, allowing resonant frequency adjustment without affecting impedance matching or passband width. Comparisons with similar designs in the literature confirm the effectiveness of the proposed method.

The paper is structured as follows. After the introduction, the design principles applied for the filter design are described in Section 2. The design requirements, optimized structure design, and results of full-wave simulations are given in Section 3. Finally, the measurements of the fabricated prototype and the results discussion are given in Section 4.

2. DESIGN PRINCIPLES

In order to discuss tunability and have a self-contained treatment, it is helpful to recall some fundamental concepts of waveguide bandpass filter design.

A waveguide band-pass filter consists of a series of resonant cavities coupled by equivalent reactive loads, typically realized by capacitive or inductive irises. The filter resonance frequency depends on the cavity lengths, which resonate at electrical lengths multiples of π, while the coupling between them primarily determines [1] the pass-band filter constitutive parameters, such as impedance matching, pass-band width, and stop-band attenuation [24]. A rigorous approach to the design is achieved through the application of the equivalent circuit model. Indeed, bandpass filters can be represented as ladder networks of alternating LC series and shunt resonators, whose values are synthesized according to the selected filter prototype (e.g., Butterworth, Chebyshev, Bessel) to obtain the desired transfer function.

In accordance with this equivalent model, the cavities correspond to series LC resonators in the equivalent circuit and are characterized by transmission line sections of length $l = \frac{\lambda_g}{2}$, where λ_g is the guided wavelength. On the other hand, the inductive/capacitive irises commonly used to connect the cavities are dimensioned to operate as impedance (admittance) inverters. These elements, modeled in the equivalent circuit model by shunt reactive loads and transmission line sections with negative equivalent length, act as quarter-wave transformers, converting shunt LC resonators into series resonators. This transmission line representation, detailed in Fig. 1, is particularly useful for evaluating the impact of design parameters on filter performance.

It is well known that the guided wavelength of a waveguide depends not only on the operating frequency, but also on both the dielectric material filling the waveguide and on the shape of the waveguide cross-section. In the specific case of a rectangular waveguide of cross-sectional dimensions $a \times b$, filled by a dielectric of relative permittivity ϵ_r, and excited by the dominant TE_{10} mode, it can be easily shown that

$$\lambda_g = \frac{\lambda_0}{\sqrt{\epsilon_r - \left(\frac{\lambda_0}{2a}\right)^2}}. \tag{1}$$

It follows that the filter-guided wavelength can be adjusted by acting on a few parameters; in turn, the resonant electrical length can also be tuned at different frequencies with respect to the nominal one.

Based on this general principle, as shown in [18], several approaches can be implemented to change the guided wavelength in a rectangular waveguide by exploiting movable walls or metal ridges. A useful approach consists of dielectric elements inserted inside the filter cavities [20, 21]. The presence of dielectric elements within the coupled cavities increases their electrical length, thus reducing the resonance frequency. This phenomenon can also be interpreted as an increase in the average dielectric permittivity of the cavity, which, according to (1), implies the decrease of λ_g. We observe a frequency shift with respect to the nominal value as the cylindrical dielectric rods are lowered inside the waveguide. The shift increases also for larger cylinder radius and/or higher relative permittivity; these parameters have been selected for the design while also taking technological constraints into account.

As an interesting variant, the use of dielectric tuning elements offers further design advantages. Compared to movable walls, good electrical contacts — which can be sometimes difficult to manufacture — are not required; moreover, compared to metallic tuning elements — which are widely used as tuning elements to compensate fabrication tolerances — they allow for an increase of the equivalent volume of material (i.e., waveguide field perturbation) that can be placed inside the filter. This potentially increases the achievable tunable range.

According to the described design guidelines, the approach followed for the design has been based on the tuning of a nominal waveguide band-pass filter — referred to for simplicity as the *reference filter* — suitably designed to satisfy the specifications at the highest frequency of the tunability range, obtained

by fully lowering the dielectric elements inside the waveguide. These elements have been dimensioned to achieve the maximum desired resonance frequency shift. However, the presence of dielectric elements also modifies the impedance of the loaded waveguide, and this implies an increasing input impedance mismatch. Therefore, it has been required to implement a matching network which is able to change its response when the tuning elements are lowered inside the cavities. For this aim, two dielectric ridges, placed at both the input and output filter ports, have been designed, which move jointly with the tuning elements and work as quarter-wavelength transformers. This way, the input impedance matching is preserved when changing the configuration.

An undesired effect that arises when the dielectric cylinders are lowered/raised is the reduction of the filter pass-band width. This phenomenon is due to the coupling irises, which, in accordance with the circuit model introduced above, have been sized to work properly as impedance inverters with respect to the maximum frequency of the tuning range and do not behave properly at different frequencies. Again, this effect increases as the shift from the nominal frequency (i.e., of the *reference filter*) increases. This problem can be overcome by using tuning elements for the irises as well, as will be detailed next.

3. FILTER DESIGN AND OPTIMIZATION

As already outlined, the proposed filter design is based on the proper modification of a *reference filter*, dimensioned to match the frequency response requirements at the maximum frequency of the considered tuning range. The requirements for this design have been defined according to standard specifications for commercial C-Band band-pass filters for SATCOM and are reported in Fig. 2. To this end, a 6^{th}-order Chebyshev filter has been designed in a standard rectangular waveguide WR-187 ($a = 47.548\,\text{mm}$ $b = 22.1488\,\text{mm}$), for which inductive irises have been exploited to implement the K-inverters [25].

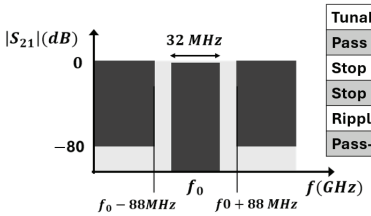

Tunable Range	f_0: [4, 4 − 5] GHz
Pass Band Width	32 MHz
Stop Band	88 *MHz* from f_0
Stop Band Attenuation	80 dB
Ripple	0, 1 dB
Pass-Band *Return Loss*	< -20 dB

FIGURE 2. Tunable filter design requirements.

Since even-order Chebyshev filters exhibit different input and output impedances, to obtain a symmetric device, an additional inductive iris has been added at the filter output [26, 27]. The dimensions of the inductive apertures and the cavity lengths have been numerically obtained according to [24, 28, 29], and then optimized by full-wave simulations. The dimensions of the designed filter elements are reported in Table 1.

The tuning elements have been inserted into the designed *reference filter*. These elements are equal-radius cylinders that can be lowered into (or raised from) filter cavities through apertures

TABLE 1. Cavity and inductive irises dimensions. The iris thickness has been set to 1 mm.

No.	Cavity Lengths $[l_{C_i}]$ (mm)	Iris Apertures $[w_{A_i}]$ (mm)
1	36.13	15.31
2	38.07	6.56
3	38.17	5.51
4	38.17	5.37
5	38.07	5.51
6	36.13	6.56
7	—	15.31

etched on the broad wall of the waveguide, aligned with the centers of the filter cavities. In this way, the resonance frequency is controlled by the depth of the dielectric cylinders within the cavities. To achieve impedance matching, two dielectric ridges have been placed outside the resonant cavities, each positioned near an outer iris. These have been designed to match the worst-case configuration, which occurs when the cylinders are fully inserted inside the cavity. Thus, a good impedance matching has been guaranteed for any cylinder configuration.

The dielectric elements are inserted into the cavities through apertures in the upper metal wall of the filter. To prevent electromagnetic field leakage, these apertures are designed as square waveguides with a small cross section (5 mm side) and a depth of 4 mm, operating under the cutoff frequency to ensure exponential field attenuation. These small apertures also guarantee proper alignment of the cylinders during assembly and operation, as their diameter is slightly smaller than the size of the aperture. The final dimensions of the ridges and the tuning elements have been achieved by full-wave simulations. The designed filter structure is finally shown in Fig. 3.

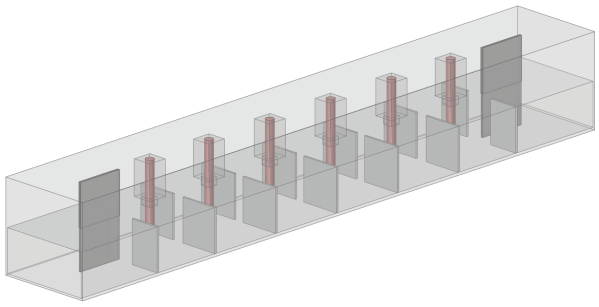

FIGURE 3. Tunable filter designed. The filter consists of six WR-187 waveguide cavities coupled by inductive irises. Tunability has been achieved through the progressive insertion of dielectric cylinders and impedance matching using movable ridges that work as quarter-wave transformers.

The cylinders employed for filter tuning have been fabricated using *alumina*, which is characterized by high power handling capability, high manufacturing precision, and relatively low losses. The latter is especially required, since the tuning cylinders are placed at the center of resonant cavities, and a strong field interaction occurs, which increases losses. According to the available datasheet, *alumina* is characterized by $\epsilon_r = 10$ and $\tan\delta = 4 \times 10^{-4}$.

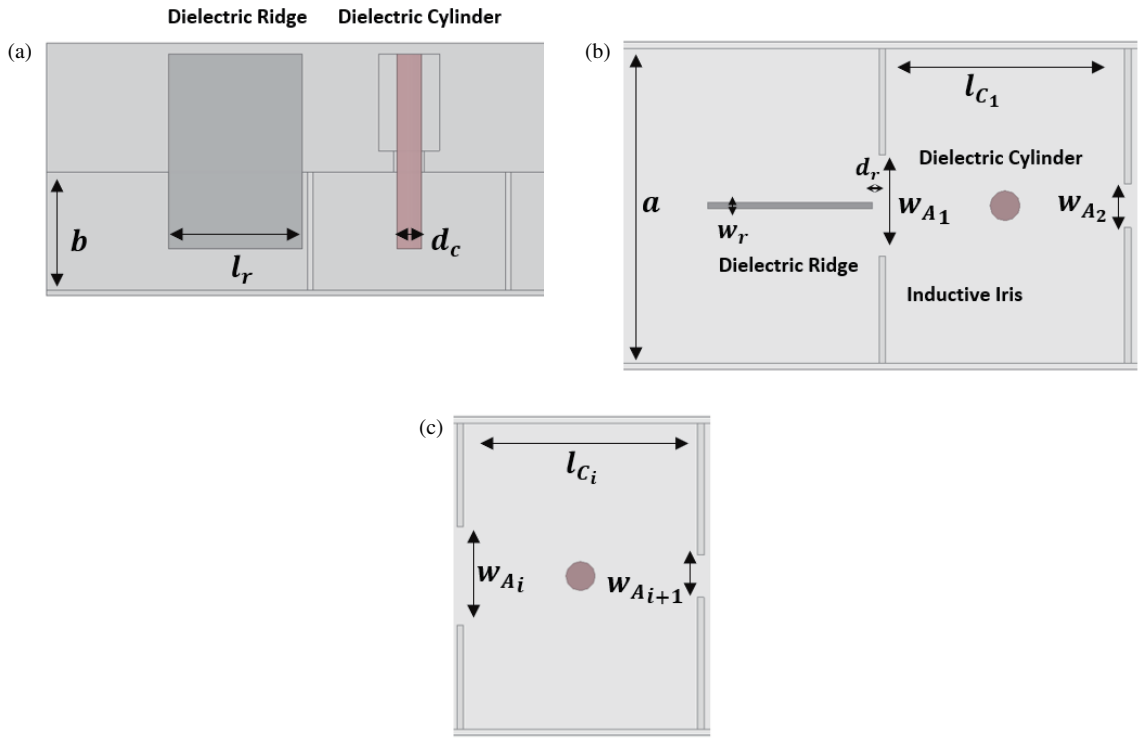

FIGURE 4. Quoted layout of the designed tunable filter. (a) Lateral view of the movable quarter-wave transformer and first filter cavity. (b) Top view of the movable quarter-wave transformer and first filter cavity. (c) Top view of the generic i-th filter cavity.

On the other hand, the ridges have been made by *Mica*, which is also a material characterized by high power handling capacity. The relative dielectric constant of *Mica* is lower than *alumina* ($\epsilon_r = 5.4$), thus allowing increased ridge thickness and simplifying mechanical realization. *Mica* is also characterized by higher dielectric losses than *alumina*; however, it does not cause a significant increase in the filter *Insertion Loss*, because they are placed outside the resonant cavities, and therefore the interaction with the field is less than in the case of cylinders in the resonant cavities. The ridges have been placed at a distance (d_R) of 0.7 mm from the filter irises (see Fig. 4). Moreover, they are characterized by a width $w_R = 1$ mm and a length $l_R = 22.5$ mm. The dielectric cylinders, with a diameter of $d_c = 4.73$ mm, penetrate 95% of the waveguide height, providing the required tuning range. Taking into account the dimensions reported above as well as those listed in Table 1, and including the input port-to-ridge spacings, the overall length is 329.40 mm.

The results of full-wave simulations, carried out with Ansys HFSS, are reported in Fig. 5 and show the frequency response of the filter at three frequencies belonging to the tunability range, namely at 4.4 GHz, 4.75 GHz, and 5 GHz. It is observed that the impedance matching is perfectly maintained for any considered configuration. Moreover, the *Insertion Loss* deteriorates when the depth of the cylinders is increased (i.e., due to a higher volume of lossy dielectrics inside the cavity), rising from 0.5 dB to a maximum of 0.8 dB.

The simulated results also show a reduction of pass-band width, from $\approx$ 32 MHz to $\approx$ 24 MHz. As anticipated, by employing additional tuning elements for the irises, this problem

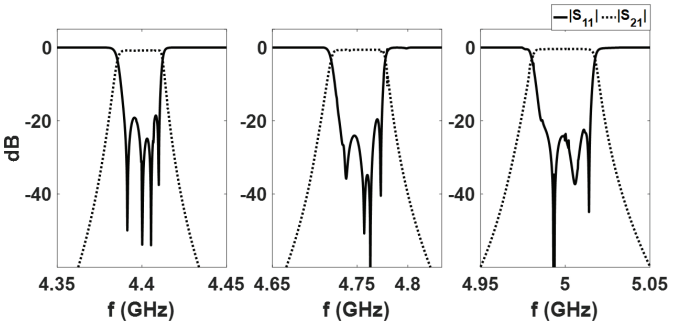

FIGURE 5. S-parameter magnitudes of the designed filter, evaluated at the three frequencies within the tuning range: 4.4 GHz, 4.75 GHz, and 5 GHz.

can be overcome. To prove this idea, the design reported in Fig. 6 has been proposed. In this example, five additional *alumina* cylinders have been inserted in correspondence with filter irises. The cylinders are identical to those used to tune the resonance frequency of filter cavities and translate together with all other movable filter elements. The results of the full-wave simulations in this project are shown in Fig. 7 and clearly demonstrate that the passband does not change at the three reference frequencies chosen within the tuning range. It is important to highlight that the implementation of these additional tuning elements does not introduce any significant mechanical complexity, as the required dielectric cylinders and the apertures on the broad wall of the waveguide are manufactured and assembled using the same process as the tuning elements employed in the filter cavities.

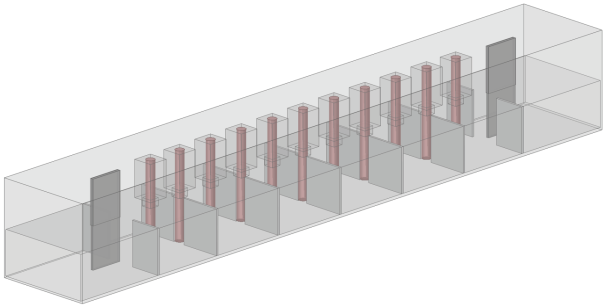

FIGURE 6. Tunable filter design including inductive iris tuning elements. These elements consist of *alumina* cylinders, equal to those used for cavity tuning, inserted between the coupling irises.

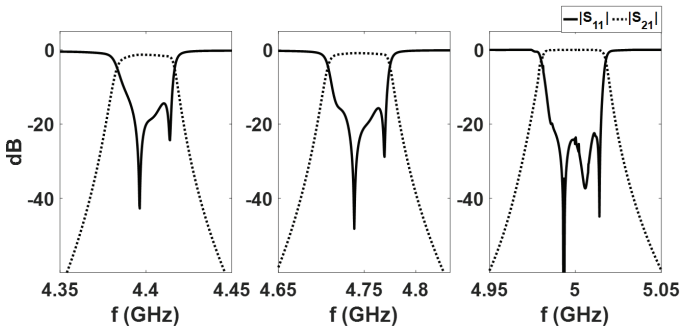

FIGURE 7. S-parameter magnitudes of the filter including inductive irises tuning elements evaluated at the three reference frequencies within the tuning range: 4.4 GHz, 4.75 GHz, and 5 GHz.

(a)

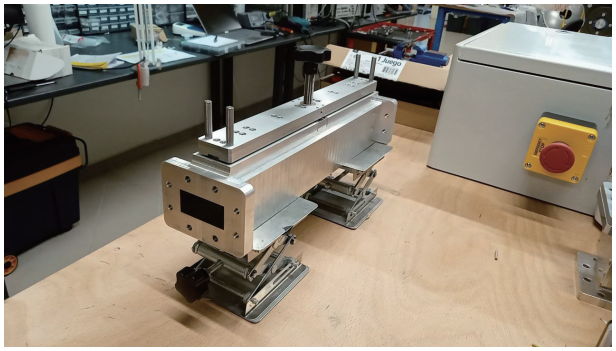

(b)

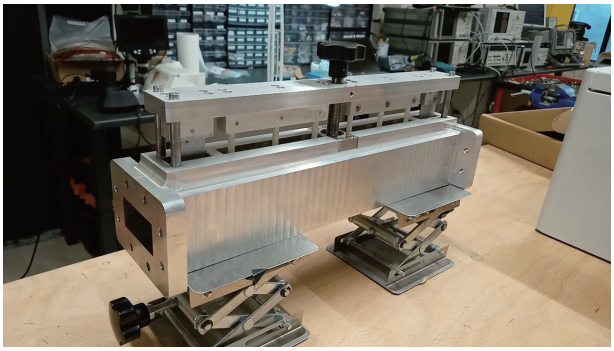

FIGURE 8. Photos of the realized tunable filter prototype. In this prototype, depth control is achieved using an endless screw that regulates the depth of the carriage for the dielectric elements inside the filter. Four metal cylinders placed at the extremities of the carriage ensure horizontal alignment.

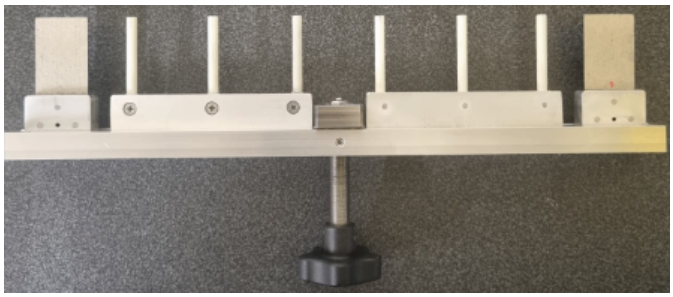

FIGURE 9. Photo of the tuning elements. The cylinders, realized in *alumina*, allow changing the resonant frequency of the cavities. The ridges, realized in *Mica*, work as quarter-wave transformers and allow impedance matching to be maintained as the resonant frequency varies.

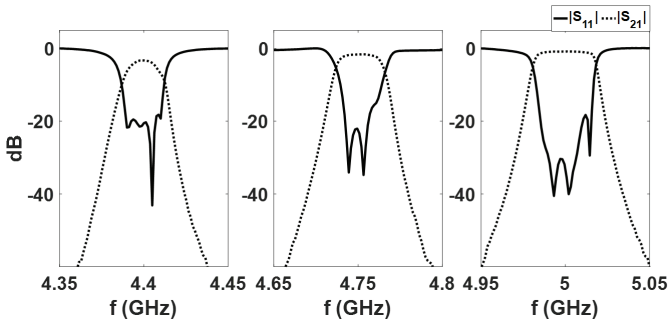

FIGURE 10. S-Parameter magnitudes measured on the prototype filter at three reference frequencies within the tuning range.

4. MEASUREMENTS AND RESULTS ANALYSIS

For the fabrication of the prototype, only the simplified design with the tuning elements for the cavities has been considered. This choice aims at simplifying the fabrication process and reducing costs; however, the results are quite general and clearly assess the performances of the proposed design. In addition, to reduce costs and ensure faster procurement, a lower-grade *alumina* has been used. The fabricated prototype is shown in Figs. 8 and 9.

The filter prototype has been experimentally characterized. The measurements, reported in Fig. 10 at the three reference frequencies, show good agreement with the simulations in terms of impedance matching. However, a higher *Insertion Loss* is observed, with $|S_{21}| < -4.1$ dB. This discrepancy is due to the actual loss tangent of *alumina*, which has been supposed to be higher than that specified in the datasheet. To verify this hypothesis, the experimental results have been compared with full-wave simulations carried out with different values of the loss tangent. As shown in Fig. 11, the measured S-parameters are in excellent agreement with the simulated ones when *alumina* is modeled with $\tan\delta = 1.8 \times 10^{-3}$. The nearly perfect match at the three reference frequencies confirms our hypothesis.

Compared to other works in the literature in which the tunability of the waveguide filter is achieved by exploiting mov-

TABLE 2. Comparison of the performance of the proposed design with designs reported in the literature, all of which utilize similar tuning technologies based on movable dielectric elements.

	Tuning Range %	BW %	Pass-Band Reduction
Proposed	12.8%	0.68%	Yes (but easily overcome)
[18]	12.8%	1.8%	Yes
[20]	6.6%	1.8%	Yes
[21]	4.6%	1.6%	No

able dielectric elements, the realized design offers higher performances in terms of tunability range and easiness of fabrication, at the price of a non-constant passband width, as shown in Table 2. This limitation can be addressed easily through the inclusion of additional tuning elements, as demonstrated by the preliminary results reported in Figs. 6 and 7.

Notably, the proposed waveguide filter has the potential to achieve low insertion loss and support high power handling through the use of high-quality *alumina*, commercially available on the market [30]. In some cases, 3D-printed *alumina* dielectric elements also exhibit very low losses [31].

For the sake of completeness, it is worth noting that high-power measurements have not been performed on the prototype, as the focus has been on demonstrating the validity of the adopted design principles. High-power handling and relative measurements typically require the use of thermal compensation systems, to prevent the effects of thermal deformation induced by the high currents flowing on filter walls [32]. Nevertheless, the materials and technology used in the design are also widely applied in high-power applications. While such measurements could be of interest to evaluate the performance of the overall system, including thermal compensation systems, they are beyond the scope of the present work.

5. CONCLUSIONS

In this paper, the design of a mechanically tunable band-pass filter in waveguide technology operating in the C-band tunability range [4.4–5] GHz, relevant for SATCOM applications, has been presented. Tunability has been achieved by inserting suitable dielectric cylinders within the filter cavities, and the impedance matching has been achieved by exploiting two identical dielectric ridges, positioned close to the filter irises, and designed to act as quarter-wave transformers. Design and optimization have been carried out by analytical and full-wave simulations. The comparison between simulated results and measurements of the first fabricated prototype demonstrates the overall good performance of the proposed device and its potential for achieving even lower insertion losses.

ACKNOWLEDGEMENTS

The authors would like to thank the European Union — Next Generation EU in the framework of projects DOSE (PRIN 2022 2022MANFK5) and IDEAS (PRIN 2022 PNRR P202293B5X).

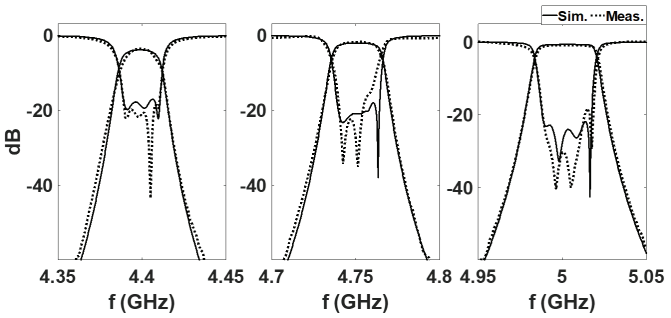

FIGURE 11. Comparison between the magnitudes of the measured and simulated S-parameters, using *alumina* characterized by $\tan\delta = 1.8\times 10^{-3}$, evaluated at three reference frequencies.

The authors express their gratitude to Concetto Squadrito, CEO of Sicilsat, for inspiring this work and supporting the filter fabrication within the framework of an ongoing collaboration between Sicilsat and the University of Catania. Davide Guarnera wishes to thank Daniel Pispisa and Salvo Laiacona for their assistance with the filter characterization.

REFERENCES

[1] Boria, V. E. and B. Gimeno, "Waveguide filters for satellites," *IEEE Microw. Mag.*, Vol. 8, No. 5, 60–70, 2007.

[2] Hunter, I., L. Billonet, B. Jarry, and P. Guillon, "Microwave filters-applications and technology," *IEEE Trans. Microw. Theory Tech.*, Vol. 50, No. 3, 794–805, 2002.

[3] Almalkawi, M., L. Zhu, and V. Devabhaktuni, "Magnetically tunable substrate integrated waveguide bandpass filters employing ferrites," in *2011 International Conference on Infrared, Millimeter, and Terahertz Waves*, 1–2, Houston, TX, USA, 2011.

[4] Laplanche, E., N. Delhote, A. Périgaud, O. Tantot, S. Verdeyme, S. Bila, D. Pacaud, and L. Carpentier, "Tunable filtering devices in satellite payloads: A review of recent advanced fabrication technologies and designs of tunable cavity filters and multiplexers using mechanical actuation," *IEEE Microw. Mag.*, Vol. 21, No. 3, 69–83, 2020.

[5] Kittel, C., "On the theory of ferromagnetic resonance absorption," *Phys. Rev.*, Vol. 73, No. 2, 155, Jan. 1948.

[6] Yang, G.-M., J. Wu, J. Lou, M. Liu, and N. X. Sun, "Low-loss magnetically tunable bandpass filters with YIG films," *IEEE Trans. Magn.*, Vol. 49, No. 9, 5063–5068, 2013.

[7] How, H., T.-M. Fang, and C. Vittoria, "Magnetic frequency-tunable millimeter-wave filter design using metallic thin films," *IEEE Trans. Microw. Theory Tech.*, Vol. 43, No. 7, 1620–1623, 1995.

[8] Hunter, I. C. and J. D. Rhodes, "Electronically tunable microwave bandpass filters," *IEEE Trans. Microw. Theory Tech.*, Vol. 30, No. 9, 1354–1360, 1982.

[9] Pelliccia, L., F. Cacciamani, P. Farinelli, and R. Sorrentino, "High-Q tunable waveguide filters using ohmic RF MEMS switches," *IEEE Trans. Microw. Theory Tech.*, Vol. 63, No. 10, 3381–3390, 2015.

[10] Shu, Y.-H., J. A. Navarro, and K. Chang, "Electronically switchable and tunable coplanar waveguide-slotline band-pass filters," *IEEE Trans. Microw. Theory Tech.*, Vol. 39, No. 3, 548–554, 1991.

[11] Yan, W. D. and R. R. Mansour, "Tunable dielectric resonator bandpass filter with embedded MEMS tuning elements," *IEEE Trans. Microw. Theory Tech.*, Vol. 55, No. 1, 154–160, 2007.

[12] Yun, T.-Y. and K. Chang, "Piezoelectric-transducer-controlled tunable microwave circuits," *IEEE Trans. Microw. Theory Tech.*, Vol. 50, No. 5, 1303–1310, 2002.

[13] Mansour, R. R., G. Basavarajappa, and S. M. Pourjaafari, "High-Q tunable bandpass filters with a wide tuning range using a minimum number of tuning elements," *IEEE Microw. Mag.*, 2–17, 2025.

[14] Widaa, A., C. Bartlett, and M. Höft, "Tunable coaxial bandpass filters based on inset resonators," *IEEE Trans. Microw. Theory Tech.*, Vol. 71, No. 1, 285–295, 2023.

[15] Widaa, A. and M. Höft, "Widely tunable TM-mode dielectric filters with constant absolute bandwidth using re-entrant caps," *IEEE Journal of Microwaves*, Vol. 3, No. 2, 706–714, 2023.

[16] Gowrish, B. and R. R. Mansour, "A tunable quarter-wavelength coaxial filter with constant absolute bandwidth using a single tuning element," *IEEE Microw. Wirel. Compon. Lett.*, Vol. 31, No. 6, 658–661, 2021.

[17] Zhou, X. and J. Huo, "Design of tunable coaxial bandpass filter based on embedded stepped impedance resonators," *IEEE Access*, Vol. 11, 58 947–58 952, 2023.

[18] Sichak, W. and H. Augenblick, "Tunable waveguide filters," *Proceedings of the IRE*, Vol. 39, No. 9, 1055–1059, 1951.

[19] Basavarajappa, G. and R. R. Mansour, "Design methodology of a tunable waveguide filter with a constant absolute bandwidth using a single tuning element," *IEEE Trans. Microw. Theory Tech.*, Vol. 66, No. 12, 5632–5639, 2018.

[20] Macchiarella, G., L. Accatino, and A. Malagoli, "Design of Ka-band tunable filters in rectangular waveguide with constant bandwidth," in *2020 IEEE Asia-Pacific Microwave Conference (APMC)*, 622–624, Hong Kong, China, 2020.

[21] Ossorio, J., V. E. Boria, and M. Guglielmi, "Dielectric tuning screws for microwave filters applications," in *2018 IEEE/MTT-S International Microwave Symposium — IMS*, 1253–1256, Philadelphia, PA, USA, 2018.

[22] De Faoite, D., D. J. Browne, F. R. Chang-Díaz, and K. T. Stanton, "A review of the processing, composition, and temperature-dependent mechanical and thermal properties of dielectric technical ceramics," *Journal of Materials Science*, Vol. 47, No. 10, 4211–4235, 2012.

[23] Vallerotonda, P., F. Cacciamani, L. Pelliccia, C. Tomassoni, and V. T. d. Crestvolant, "High-power ka-band bandpass filter based on movable dielectric-loaded TE01δ mode resonators," in *2022 52nd European Microwave Conference (EuMC)*, 111–114, Milan, Italy, 2022.

[24] Matthaei, L., G. L. Young, and E. M. T. Jones, *Microwave Filters, Impedance Matching Networks and Coupling Structures*, Artech Microwave Library, 1964.

[25] Pozar, D. M., *Microwave Engineering: Theory and Techniques*, John Wiley & Sons, 2021.

[26] Zhang, S. and L. Zhu, "General synthesis method for symmetrical even-order Chebyshev bandpass filter," in *2012 Asia Pacific Microwave Conference Proceedings*, 667–669, Kaohsiung, Taiwan, 2012.

[27] Yang, J., L. Cui, C. Chen, and W. Wu, "Synthesis of symmetrical even-order Chebyshev filters," in *2008 Asia-Pacific Microwave Conference*, 1–4, Hong Kong, China, 2008.

[28] Collin, R. E., *Foundations for Microwave Engineering*, John Wiley & Sons, 2007.

[29] Rizzi, P. A., *Microwave Engineering: Passive Circuits*, Prentice Hall New Jersey, 1988.

[30] Kyocera Global, "High-purity alumina (AO479U) for microwave applications," [Online]. Available: https://global.kyocera.com/prdct/fc/technologies/013.html, 2025.

[31] Jiménez-Sáez, A., M. Schüßler, C. Krause, D. Pandel, K. Rezer, G. V. Bögel, N. Benson, and R. Jakoby, "3D printed alumina for low-loss millimeter wave components," *IEEE Access*, Vol. 7, 40 719–40 724, 2019.

[32] Guarnera, D., G. S. Mauro, S. C. Pavone, T. Isernia, and G. Sorbello, "Multiphysics analysis of thermal deformation effects on a waveguide bandpass filter," *IEEE Access*, Vol. 13, 71 447–71 455, 2025.